Inorganic Chemistry

pubs.acs.org/IC Article

Long-Lived Photoluminescence of Molecular Group 14 Compounds through Thermally Activated Delayed Fluorescence

Anitha S. Gowda, Tia S. Lee, Michael C. Rosko, Jeffrey L. Petersen, Felix N. Castellano,* and Carsten Milsmann*

Cite This: https://doi.org/10.1021/acs.inorgchem.2c00182 Read Online

ACCESS | Metrics & More | Article Recommendations | Supporting Information

ABSTRACT: Photoluminescent molecules exploiting the sizable spin−orbit coupling constants of main group metals and metalloids to access long-lived triplet excited states are relatively rare compared to phosphorescent transition metal complexes. Here we report the synthesis of three air- and moisture-stable group 14 compounds $E(^{Me}PDP^{Ph})_2$, where E = Si, Ge, or Sn and $[^{Me}PDP^{Ph}]^{2-}$ is the doubly deprotonated form of 2,6-bis(5-methyl-3-phenyl-1*H*-pyrrol-2-yl)pyridine. In solution, all three molecules exhibit exceptionally long-lived triplet excited states with lifetimes in the millisecond range and show highly efficient photoluminescence ($\Phi \leq 0.49$) due to competing prompt fluorescence and thermally activated delayed fluorescence at and around room temperature. Temperature-dependent steady-state emission spectra and photoluminescent lifetime measurements provided conclusive evidence for the two distinct emission pathways. Picosecond transient absorption spectroscopy allowed further analysis of the intersystem crossing (ISC) between singlet and triplet manifolds (τ_{ISC} = 0.25−3.1 ns) and confirmed the expected trend of increased ISC rates for the heavier elements in otherwise isostructural compounds.

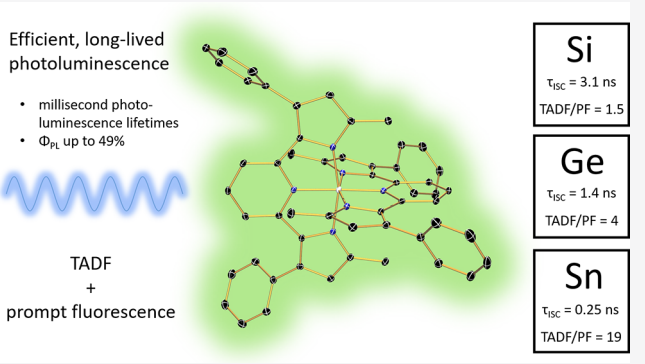

INTRODUCTION

Molecular chromophores with long-lived excited states are at the center of many important technological innovations, including photocatalysis,[1−4] photodynamic therapy,[5] chemo- and biosensing,[6] dye-sensitized solar cells,[7,8] and organic light-emitting diodes (OLEDs).[9−11] Many advances in these areas continue to rely on the unique properties of photoluminescent transition metal complexes allowing excitations through metal-to-ligand charge transfer (MLCT), ligand-to-metal charge transfer (LMCT), or d−d transitions.[12−15] The key feature leading to the success of these compounds is efficient intersystem crossing (ISC) facilitated by the metal center, which enables the population of excited states with spin multiplicities different from those of the corresponding ground states, resulting in spin-forbidden, slow radiative relaxation by phosphorescence or thermally activated delayed fluorescence (TADF).[16] The prerequisite of fast ISC provides a rationale for the predominance of heavy, and often rare and precious, second- and third-row transition metals, which exhibit large spin−orbit coupling (SOC) constants. These precious metal photosensitizers are most prominently represented by ruthenium polypyridyl complexes[17] and organometallic iridium compounds.[18,19] However, the low availability and the associated high costs of these metals represent significant economic barriers for potential large scale applications.

While substantial progress toward the use of more Earth-abundant transition metal chromophores has been made recently,[13,20−22] main group compounds featuring long-lived emissive states at room temperature remain rare even though they could also provide abundant and cost-efficient alternatives to precious metal chromophores.[23,24] Organic materials exhibiting room-temperature phosphorescence or TADF have become an intensively explored topic but typically require aggregation or self-assembly through noncovalent interactions (e.g., hydrogen or halogen bonding), formation of polymeric structures, or crystallization to minimize nonradiative decay.[25−32] Despite recent progress toward the rational design of heavy atom-free triplet photosensitizers,[33−38] the most common strategy for improving the otherwise slow ISC rates in organic chromophores is to exploit intra- or intermolecular heavy atom effects. In some instances, the incorporation of the heavy halogens bromine and iodine into rigid molecular structures has allowed the preparation of organic chromo-

Received: January 18, 2022

https://doi.org/10.1021/acs.inorgchem.2c00182
Inorg. Chem. XXXX, XXX, XXX−XXX

phores with long-lived emission at room temperature even in solution.[39] Beyond halogens, examples of long-lived emission from molecules incorporating main group metals or metalloids are even scarcer, although these heavy main group elements also display strong SOC that should accelerate ISC.[40] Early examples for phosphorescence from molecules containing heavy group 14 and 15 elements (Sb, Bi, Sn, and Pb) showed that these elements can play a key role in enhancing access to ligand-centered $\pi \rightarrow \pi^*$ triplet states.[41−44] Enhanced ISC rates yielding long-lived triplet states were also established for tin(IV) porphyrin compounds.[45−47] The resulting triplet excited states were subsequently shown to decay through a combination of phosphorescence and TADF and have been utilized for triplet exciton harvesting in electroluminescent devices.[46] More recent research efforts have focused on heavy elements with s^2 electron configurations[48−51] such as lead(II), tin(II), and bismuth(III) or chalcogen compounds like tellurophenes,[52−55] which show intense phosphorescence under ambient conditions in the solid state. Examples implementing lighter main group elements of the second and third period such as boron, phosphorus, and sulfur in molecules with long-lived emission are known but remain exceedingly rare and often require aggregation or self-assembly to access triplet manifolds.[24]

In the context of our ongoing research efforts in developing photosensitizers based on Earth-abundant elements, we recently reported the photoluminescent properties of zirconium complexes with pyridine pyrrolide and pyridine dipyrrolide (PDP) ligands.[56−60] $Zr(PDP)_2$ complexes show remarkably long-lived and quantum-efficient emission by TADF involving energetically close-lying singlet and triplet excited states with strongly mixed LMCT/intraligand (IL) character.[61] We hypothesized that replacing the central Zr^{IV} center with a tetravalent group 14 element would allow us to produce main group chromophores with efficient ISC to long-lived triplet excited states (Figure 1). Precedent for enhanced ISC rates in group 14 compounds with polypyrrole-type ligands was provided by the tin porphyrin compounds mentioned above, which can access triplet states in the solid state and in solution.[45−47] Further inspiration was provided by a series of Sn^{IV} and Pb^{IV} compounds reported by Wang and co-workers containing bis(indolyl)pyridine ligands, which are closely related to the pyridine dipyrrolide framework.[42] These compounds exhibit phosphorescence with microsecond lifetimes, albeit only in frozen solution at 77 K.

Herein, we report three photoluminescent molecules $E(^{Me}PDP^{Ph})_2$ (E = Si, Ge, or Sn), where $[^{Me}PDP^{Ph}]^{2-}$ is the doubly deprotonated form of 2,6-bis(5-methyl-3-phenyl-1*H*-pyrrol-2-yl)pyridine. All three compounds readily access triplet states upon photoexcitation at room temperature in solution. Temperature-dependent emission studies clearly establish that the long-lived luminescence is dominated by TADF at and around room temperature. A comparison of the ISC rates determined through femtosecond transient absorption (fs-TA) spectroscopy shows a clear trend favoring elements with higher atomic numbers and larger spin−orbit coupling constants. Most importantly, the observation of long-lived luminescence for $Si(^{Me}PDP^{Ph})_2$ highlights the fact that fast ISC rates competitive with excited-state decay by prompt fluorescence and nonradiative processes can be achieved under ambient conditions in solution without the incorporation of elements beyond the third period.

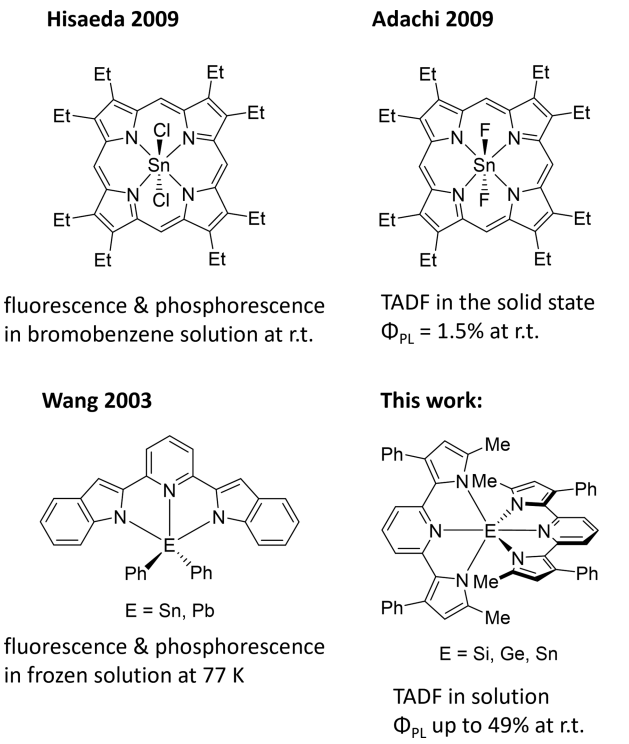

Figure 1. Examples of luminescent group 14 polypyrrole compounds that can access long-lived triplet excited states upon photoexcitation.

RESULTS AND DISCUSSION

Synthesis and Characterization of Group 14 Bis-$^{Me}PDP^{Ph}$ Complexes. The three $E(^{Me}PDP^{Ph})_2$ compounds (E = Si, Ge, or Sn) were obtained via a straightforward synthetic protocol from the reaction of the corresponding tetrahalides and 2 equiv of $Na_2{}^{Me}PDP^{Ph}$, prepared *in situ* by deprotonation of 2,6-bis(5-methyl-3-phenyl-1*H*-pyrrol-2-yl)-pyridine, $H_2{}^{Me}PDP^{Ph}$ (Scheme 1). All three compounds were

Scheme 1. Synthesis of Group 14 $E(^{Me}PDP^{Ph})_2$ Compounds

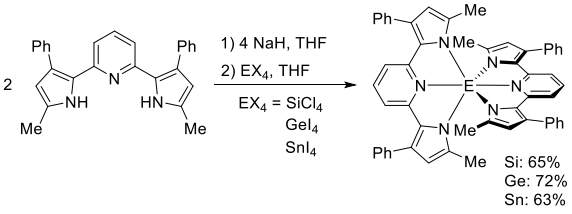

isolated as solvates following recrystallization from either THF/pentane, $E(^{Me}PDP^{Ph})_2{\cdot}2THF$, or dichloromethane/pentane, $E(^{Me}PDP^{Ph})_2{\cdot}3CH_2Cl_2$. Because most experiments discussed in this work were conducted in solution and probed molecular properties of the group 14 species under those conditions, we will omit co-crystallized solvent molecules throughout the text. However, solvent molecules were considered as part of the molecular formula for all measurements relying on accurate concentrations of the group 14 species. In contrast to their transition metal congeners, all three group 14 species are stable to air and moisture as solids and in solution (Figure S9). This can most likely be attributed to the increased covalency of the E−N bonds and the shorter E−N bond lengths (*vide infra*) that result in increased levels of steric protection around the central atom.

https://doi.org/10.1021/acs.inorgchem.2c00182
Inorg. Chem. XXXX, XXX, XXX−XXX

Characterization by single-crystal X-ray diffraction analysis established isostructural molecules with six-coordinate group 14 centers in distorted octahedral coordination environments (see Figure 2 for Si and Figures S1 and S2 for Ge and Sn,

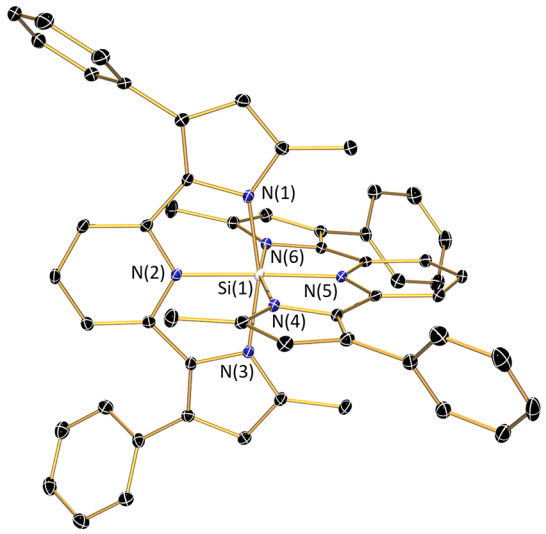

Figure 2. Molecular structure of Si(^{Me}PDP^{Ph})$_2$ obtained by X-ray diffraction shown with 30% probability ellipsoids. Hydrogen atoms and two co-crystallized molecules of THF have been omitted for the sake of clarity.

respectively). For Si(^{Me}PDP^{Ph})$_2$·2THF, the central silicon atom lies on the crystallographic C_2 axis of the $C2/c$ unit cell, which renders the two ^{Me}PDP^{Ph} ligands equivalent. For the Ge and Sn analogues, which crystallize in the $P\bar{1}$ space group with three molecules of dichloromethane per asymmetric unit, no such symmetry is present, resulting in crystallographically distinct ^{Me}PDP^{Ph} moieties albeit with nearly identical geometric parameters. The planes defined by the two pincer ligands are arranged almost perpendicular in all compounds, and the N_{py}–E–N_{py} angles are close to 180° (Table 1). The most significant deviation from an ideal octahedral geometry is introduced by the small bite angles of the ^{Me}PDP^{Ph} framework, which do not permit a perfect *trans* orientation of the pyrrolide units. This distortion becomes more prominent with the increasing atomic radius of the central element (Si < Ge < Sn),

Table 1. Selected Bond Distances (angstroms) and Angles (degrees) in E(^{Me}PDP^{Ph})$_2$ (E = Si, Ge, or Sn)

	Si(^{Me}PDP^{Ph})$_2$	Ge(^{Me}PDP^{Ph})$_2$	Sn(^{Me}PDP^{Ph})$_2$
E–N(1)	1.9071(13)	1.977(3)	2.1269(19)
E–N(2)	1.8523(11)	1.954(3)	2.1605(17)
E–N(3)	1.8904(13)	1.993(3)	2.1154(19)
E–N(4)[a]		1.988(3)	2.1231(18)
E–N(5)[a]		1.956(3)	2.1534(17)
E–N(6)[a]		1.976(3)	2.1405(19)
N(2)–E–N(5)	175.96(8)	176.80(11)	173.53(7)
N(1)–E–N(3)	165.30(5)	160.96(11)	149.91(7)
N(4)–E–N(6)[a]		160.78(11)	150.60(7)
θ_d[b]	89.13	89.62	88.64

[a]For Si(^{Me}PDP^{Ph})$_2$, crystallographic symmetry renders the two ^{Me}PDP^{Ph} ligands identical. [b]Dihedral angle between the planes defined by the nitrogen donors of each pincer ligand.

which results in longer E–N_{py} bonds and decreases the $N_{pyrrole}$–E–$N_{pyrrole}$ angles for each ligand (Table 1).

The ^{1}H and ^{13}C{^{1}H} NMR spectroscopic data for all three compounds show 7 and 12 distinct resonances, respectively, consistent with D_{2d} symmetric structures on the NMR time scale in a dichloromethane-d_2 solution (Figures S3–S8). For Sn(^{Me}PDP^{Ph})$_2$, J coupling between the Sn center (^{117}Sn, 7.7% natural abundance, and ^{119}Sn, 8.6% natural abundance; both I = $^1/_2$) and the protons on the pyridine and pyrrolide rings can be observed, indicating significant magnetic interactions mediated by the ^{Me}PDP^{Ph} framework.

Steady-State Electronic Absorption and Emission Spectroscopy. The electronic absorption spectra for Si(^{Me}PDP^{Ph})$_2$, Ge(^{Me}PDP^{Ph})$_2$, and Sn(^{Me}PDP^{Ph})$_2$ recorded in THF solutions (Figure 3) are remarkably similar, indicating

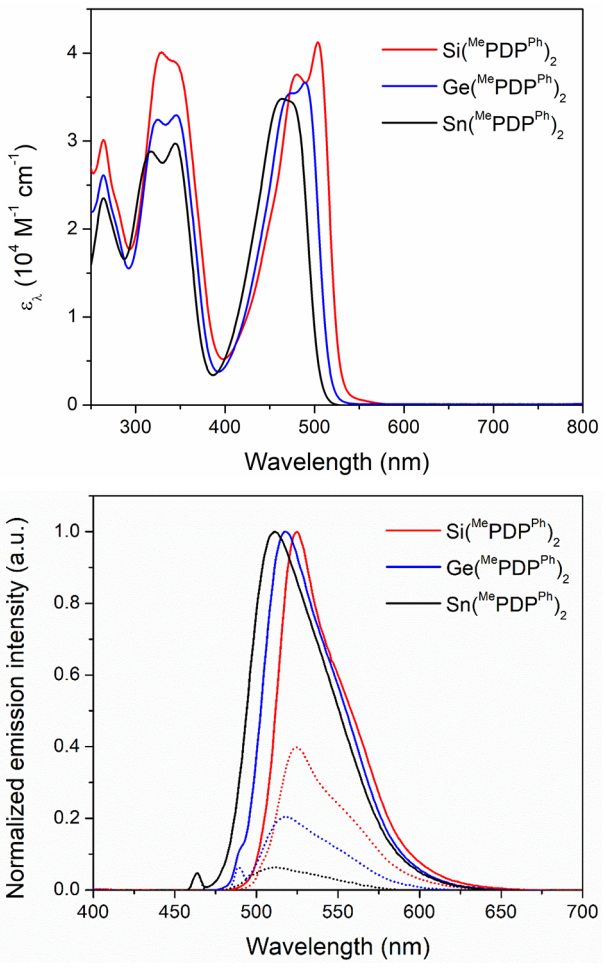

Figure 3. Optical properties of E(^{Me}PDP^{Ph})$_2$ [E = Si (red), Ge (blue), or Sn (black)]. The top panel shows electronic absorption spectra in THF solution at room temperature, and the bottom panel emission spectra recorded in THF at room temperature under a N_2 atmosphere (solid line) and in an aerated solution (dotted line) upon excitation at 460 nm (Sn), 490 nm (Ge), or 500 nm (Si).

only small contributions of the central element to the frontier molecular orbitals of the compounds. This is supported by DFT calculations that show only minimal contributions from the central element to the frontier molecular orbitals [<1% for HOMO to HOMO−3 and <3% for LUMO to LUMO+3 (Figures S17–S19)]. All three complexes show strong absorption bands ($\varepsilon_{\lambda,max}$ > 10^4 M^{-1} cm^{-1}) between 400 and

https://doi.org/10.1021/acs.inorgchem.2c00182
Inorg. Chem. XXXX, XXX, XXX–XXX

550 nm. For Si(^{Me}PDP^{Ph})$_2$, two clearly resolved maxima are observed at 504 and 480 nm. Incorporation of the heavier elements Ge and Sn results in a slight but systematic blue shift across the series, a reduction in the peak separation for Ge(^{Me}PDP^{Ph})$_2$ (490 and 473 nm), and a single broad band for Sn(^{Me}PDP^{Ph})$_2$ (476–461 nm). Several additional spectral features of similar intensity can be observed in the UV region of the spectrum (Table 2). Notably, the two absorption bands between 300 and 400 nm show a similar albeit less pronounced trend of blue-shifted peak maxima with an increase in atomic number. However, the peak separation between the two absorption maxima increases for the heavier elements, establishing a reverse trend compared to the bands in the visible region.

Table 2. Optical Properties of E(^{Me}PDP^{Ph})$_2$ (E = Si, Ge, or Sn)

compound[a]	absorption λ_{max} (nm) [ε_λ ($\times 10^4$ M^{-1} cm^{-1})]	emission λ_{max} (nm)	Φ_{PL}	τ (ms)
Si(^{Me}PDP^{Ph})$_2$	504 (4.12), 480 (3.75), 344 (3.90), 328 (4.00), 264 (3.01)	527	0.47	0.9
Ge(^{Me}PDP^{Ph})$_2$	490 (3.66), 473 (3.54), 345 (3.29), 325 (3.24), 264 (2.61)	519	0.49	1.0
Sn(^{Me}PDP^{Ph})$_2$	464 (3.47), 344 (2.97), 317 (2.88), 264 (2.35)	512	0.32	2.0

[a]All data recorded in THF solutions at room temperature.

Excitation of Si/Ge/Sn(^{Me}PDP^{Ph})$_2$ solutions in THF under an inert atmosphere with visible light below 500 nm or UV light induced strong photoluminescence (Figure 3) with peak maxima at 527, 519, and 512 nm, respectively. All three emission signals show slightly asymmetric profiles, which are likely due to unresolved vibrational fine structure. Mirroring the differences in peak separation of the lowest-energy features in the absorption spectra, this asymmetry is most clearly observable for Si(^{Me}PDP^{Ph})$_2$, which exhibits the smallest line width and features a distinct shoulder around 553 nm. Emission quantum yields were determined by the comparative method in a rigorously deaerated THF solution (Figure S11), which provided Φ_{PL} values of 0.47 (Si), 0.49 (Ge), and 0.32 (Sn). Additional steady-state emission spectra recorded in air-saturated THF solutions under otherwise identical conditions showed marked reductions in the emission intensities for all three compounds. Comparisons of the emission spectra under air and an inert atmosphere, recorded on the same sample for each compound, are shown in Figure 3 and clearly establish partial photoluminescence quenching by $^3O_2$. Notably, the extent of quenching depends strongly on the central element.

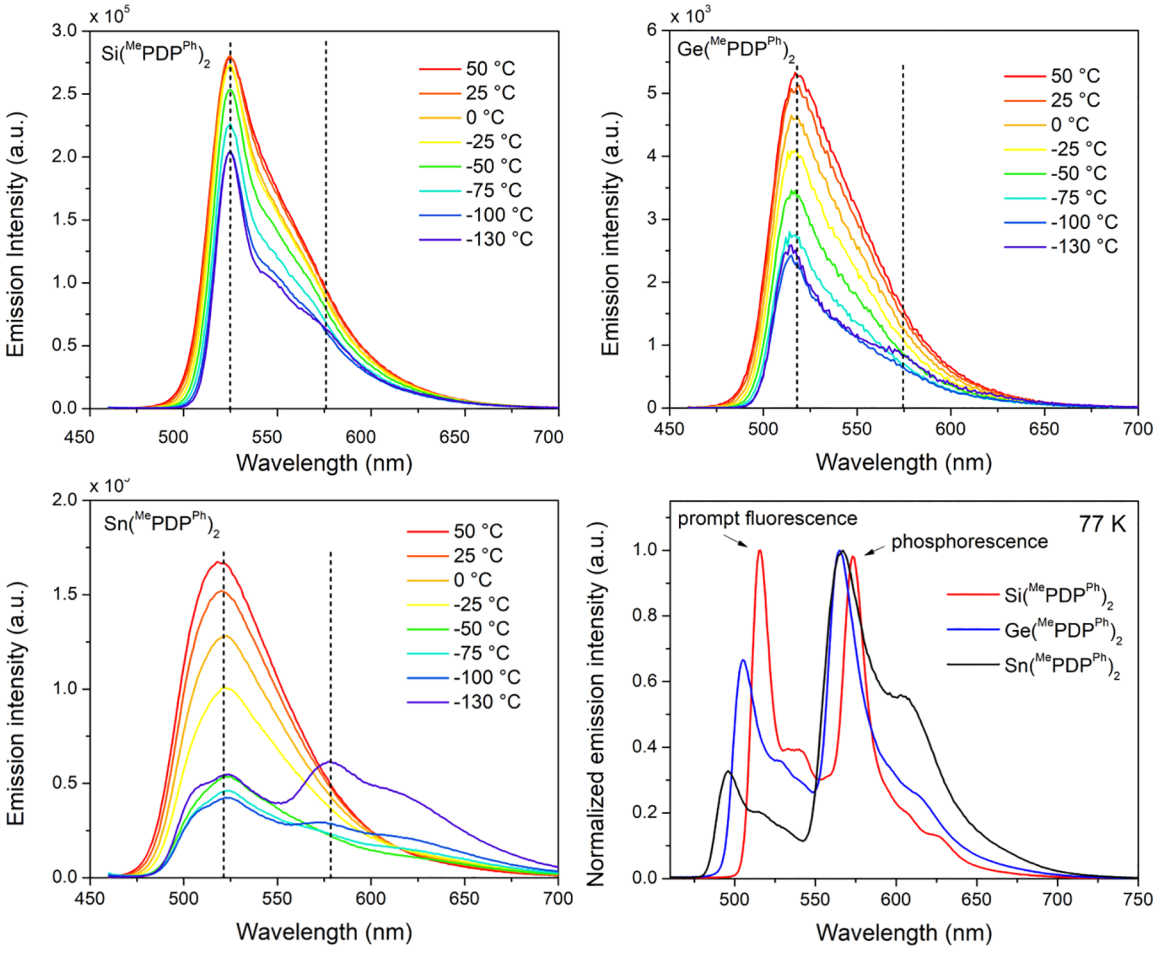

Figure 4. Temperature dependence of the emission spectra for Si(^{Me}PDP^{Ph})$_2$ (top left), Ge(^{Me}PDP^{Ph})$_2$ (top right), and Sn(^{Me}PDP^{Ph})$_2$ (bottom left) in 2-MeTHF solution upon excitation at 450 nm. Dotted vertical lines mark the position of the emission maximum for fluorescence at 50 °C and phosphorescence at −130 °C. The emission profiles in frozen solution at 77 K are shown at the bottom right.

https://doi.org/10.1021/acs.inorgchem.2c00182
Inorg. Chem. XXXX, XXX, XXX−XXX

While 40% of the signal intensity recorded under a N_2 atmosphere is retained for aerated samples of Si(^{Me}PDP^{Ph})$_2$, only 20% and 5% of their initial intensities are obtained in the presence of $^3O_2$ for the Ge and Sn congeners, respectively. The formation of $^1O_2$ was confirmed by detection of the characteristic $^1O_2$ phosphorescence around 1280 nm upon photoexcitation of aerated THF solutions of Si/Ge/Sn-(^{Me}PDP^{Ph})$_2$ at 480 nm. Quantitative analysis of the $^1O_2$ sensitization compared to [Ru(bpy)$_3$](PF$_6$)$_2$ as the standard provided quantum yields of 0.09, 0.10, and 0.12 for Si, Ge, and Sn, respectively (Figure S12). These data are consistent with more efficient triplet formation with the heaviest element Sn.

Independent of the central atom, the position and line shape of the emission spectra for all three species are insensitive to the presence of $^3O_2$, and normalization of the spectra under an inert atmosphere and air yields superimposable profiles. These observations are consistent with two distinct emission processes, which were tentatively assigned as rapid prompt fluorescence, unaffected by $^3O_2$, and photoluminescence involving a long-lived triplet excited state that is strongly quenched by $^3O_2$. The correlation between the quenching efficiency and the atomic number of the central group 14 element supports the participation of triplet states, as increased SOC in the heavier elements should facilitate ISC between singlet and triplet excited-state manifolds. However, the identical emission profiles in the presence and absence of $^3O_2$ further suggest that both photoluminescence processes emanate from the same excited state at room temperature. This rules out direct emission from the triplet excited state by phosphorescence and indicates TADF for all three E-(^{Me}PDP^{Ph})$_2$ compounds, as also observed in the closely related transition metal photosensitizer Zr(^{Mes}PDP^{Ph})$_2$.

Temperature-dependent emission spectra were recorded to further probe the photoluminescence mechanism in Si/Ge/Sn(^{Me}PDP^{Ph})$_2$ and are shown in Figure 4. Consistent with the TADF hypothesis, the emission profiles recorded in fluid 2-MeTHF between 50 and −130 °C show a steady decrease in intensity with a decrease in temperature characteristic of contributions from a thermally activated emission process. The most prominent changes were observed for Sn(^{Me}PDP^{Ph})$_2$. The broad high-temperature emission band (λ_{max} = 522 nm) undergoes a substantial reduction in intensity upon cooling, accompanied by the emergence of a red-shifted emission feature with a maximum at 580 nm, which is clearly resolved at temperatures below −100 °C. This behavior can readily be explained by emission from two distinct but energetically close-lying excited states that were assigned as S_1 and T_1 assuming a typical TADF model. The emission spectrum of Sn(^{Me}PDP^{Ph})$_2$ at −130 °C, the lowest temperature maintaining a fluid solution, is dominated by phosphorescence from the T_1 state with a λ_{max} of 580 nm but retains a minor contribution from prompt fluorescence at a λ_{max} of 522 nm due to incomplete ISC. At higher temperatures, reverse intersystem crossing (rISC) becomes thermodynamically feasible, resulting in dominant emission from the S_1 state through a combination of prompt fluorescence and TADF.

Less pronounced but qualitatively similar behavior was observed for the temperature-dependent emission in Ge-(^{Me}PDP^{Ph})$_2$. The emission profile shows a significant reduction in intensity of the main emission band at a λ_{max} of 519 nm upon cooling and evolution of a new red-shifted signal at a λ_{max} of 575 nm attributed to phosphorescence. The higher ratio of fluorescence to phosphorescence in Ge(^{Me}PDP^{Ph})$_2$ compared to Sn(^{Me}PDP^{Ph})$_2$ at −130 °C supports less efficient triplet excited-state population by ISC, which is consistent with the results from $^3O_2$ quenching at room temperature (*vide supra*) and further supported by TA spectroscopy (*vide infra*). In line with this interpretation, even more moderate changes to the emission spectrum upon cooling were observed for Si-(^{Me}PDP^{Ph})$_2$. A modest decrease in emission intensity at a λ_{max} of 525 nm is accompanied by only minor changes to the overall shape of the emission band even at −130 °C. Consistent with more pronounced prompt fluorescence due to slow ISC, the phosphorescence signal can barely be observed as a shoulder in the emission profile around a λ_{max} of 575 nm at this temperature.

Frozen solution emission spectra obtained upon further cooling to 77 K establish clearly resolved dual emission by fluorescence and phosphorescence for all three compounds and provide evidence for competing prompt fluorescence and ISC processes following photoexcitation. The normalized spectra shown in Figure 4 highlight the differences in the relative intensity of fluorescence and phosphorescence within the series, where prompt fluorescence decreases with an increase in the atomic number of the main group element. This trend is consistent with the $^3O_2$ quenching data that suggested more efficient population of the triplet excited state in the following order: Sn(^{Me}PDP^{Ph})$_2$ > Ge(^{Me}PDP^{Ph})$_2$ > Si-(^{Me}PDP^{Ph})$_2$. Additionally, the frozen solution data allow an estimation of the energy gap between the S_1 and T_1 states, $\Delta E_{S_1-T_1}$, by comparison of the emission maxima and provided values of 1958 cm^{-1} (Si), 2095 cm^{-1} (Ge), and 2524 cm^{-1} (Sn). Notably, this increase in $\Delta E_{S_1-T_1}$ with the atomic number of the central element is driven largely by a blue shift of the fluorescence band, i.e., an increase in the energy of the S_1 state. In contrast, the energy of T_1 remains largely unchanged among the three compounds as indicated by almost identical emission wavelengths for phosphorescence in liquid and frozen solutions. This may be the result of increased charge transfer character for the S_1 state compared to the T_1 state, which is supported by TD-DFT calculations. Figure 5 shows the

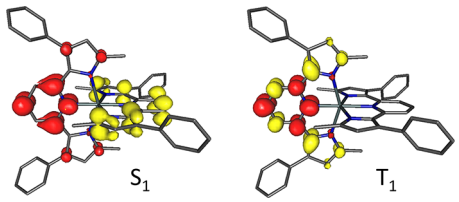

Figure 5. Difference densities for the lowest-energy singlet (^{1}LLCT, left) and triplet (^{3}LC, right) states (red, increase in electron density; yellow, decrease in electron density). Note that due to the D_{2d} symmetric molecular structure, both states are degenerate with areas of increased and decreased density located on the other ^{Me}PDP^{Ph} ligand.

difference densities for both states with respect to the ground state for Sn(^{Me}PDP^{Ph})$_2$ (see Figures S20 and S21 for the Si and Ge analogues) and clearly indicates ligand-to-ligand charge transfer (^{1}LLCT) character for the S_1 state. Due to the increase in E−N bond lengths within the series E = Sn > Ge > Si, the polarity of the S_1 state increases for the heavier elements, resulting in larger thermally induced Stokes shifts. In contrast, the T_1 state is largely ligand centered (^{3}LC) and nonpolar, making it less sensitive to the identity of the central element.

https://doi.org/10.1021/acs.inorgchem.2c00182
Inorg. Chem. XXXX, XXX, XXX−XXX

Time-Resolved Emission Spectroscopy. The photoluminescence decay traces for Si(^{Me}PDP^{Ph})$_2$, Ge(^{Me}PDP^{Ph})$_2$, and Sn(^{Me}PDP^{Ph})$_2$ in THF solution are shown in Figure 6 and

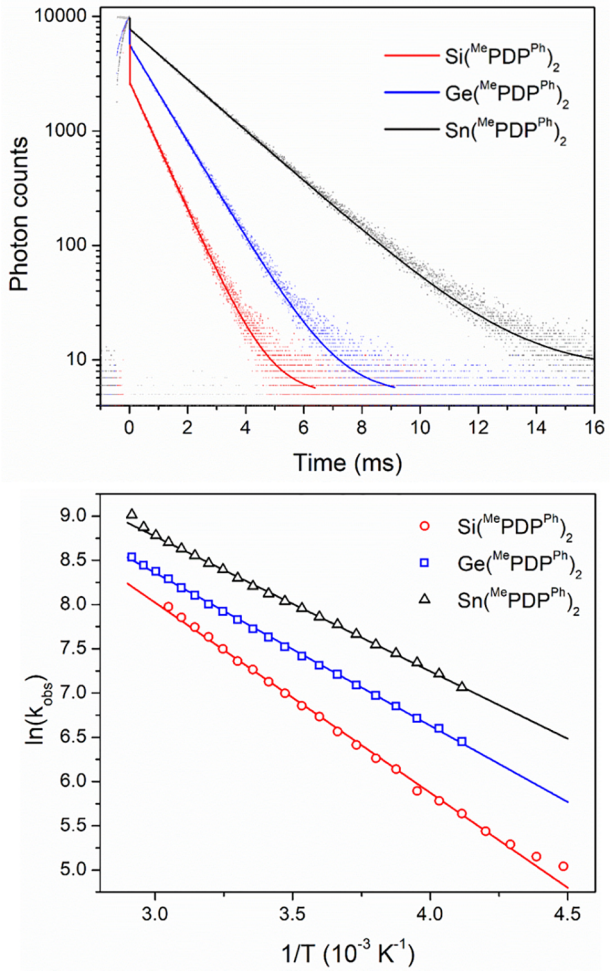

Figure 6. Photoluminescence decay (top) at room temperature in a THF solution (λ_{ex} = 456 nm). Solid lines represent exponential fits of the data. Arrhenius plot (bottom) showing the temperature dependence of the photoluminescence lifetime ($\tau = 1/k_{obs}$) in 2-MeTHF. Solid lines show best fits to the data and provided the following activation energies for TADF emission: E_a(Si) = 1493 cm^{-1}, E_a(Ge) = 1201 cm^{-1}, and E_a(Sn) = 1061 cm^{-1}.

support two distinct emission processes occurring on vastly different time scales. For all three compounds, a rapid decrease in luminescence intensity is observed immediately after excitation and can be assigned to prompt fluorescence (τ_{PF} < 2 ns). Consistent with the steady-state emission intensities obtained under an inert atmosphere and in the presence of air, the amount of prompt fluorescence is largest for Si(^{Me}PDP^{Ph})$_2$ and decreases gradually for Ge(^{Me}PDP^{Ph})$_2$ and Sn(^{Me}PDP^{Ph})$_2$. In addition to prompt fluorescence, a second, long-lived emission signal representing delayed fluorescence is observed in each case and follows strictly single-exponential decay with a millisecond lifetime (Table 2). Exposure of the samples to air resulted in complete quenching of this long-lived emission.

Temperature-dependent photoluminescence lifetime measurements for the long-lived emission feature provided further support for a TADF mechanism in Si/Ge/Sn(^{Me}PDP^{Ph})$_2$ (Figure S13). For each compound, the photoluminescence lifetime in a 2-MeTHF solution increases as a function of a decrease in temperature, clearly indicating thermal activation of emission. A simple Arrhenius-type plot (Figure 6) was used to determine the activation energy of delayed fluorescence for each compound and provided the following values: E_a(Si) = 1493 cm^{-1}, E_a(Ge) = 1201 cm^{-1}, and E_a(Sn) = 1061 cm^{-1}. Notably, these energy barriers not only are significantly smaller than the $\Delta E_{S_1-T_1}$ values derived from the frozen solution emission spectra (*vide supra*) but also exhibit the reverse trend within the series of group 14 species. While E_a^{TADF} and $\Delta E_{S_1-T_1}$ are often close for TADF emitters and generally follow the relation $\Delta E_{S_1-T_1} \geq E_a^{TADF}$, cases with significant deviations such as those presented here are not uncommon but indicate more complex dynamics in the excited-state manifold.[62,63] A more detailed analysis of the excited-state manifold in Si/Ge/Sn(^{Me}PDP^{Ph})$_2$ is beyond the scope of this initial report and will require more in-depth photophysical studies of these novel group 14 TADF emitters.

Transient Absorption Spectroscopy. The simultaneous observation of prompt fluorescence and TADF strongly implied that intersystem crossing from the singlet to the triplet manifold ($S_1 \rightarrow T_n$) and direct singlet deactivation ($S_1 \rightarrow S_0$) following photoexcitation have to be competitive processes in Si/Ge/Sn(^{Me}PDP^{Ph})$_2$. To experimentally determine the ISC rate constants, femtosecond transient absorption (fs-TA) experiments were conducted at room temperature (Sn in Figure 7 and Si and Ge in Figures S14 and S15). For all three E(^{Me}PDP^{Ph})$_2$ compounds (E = Si, Ge, or Sn), the transient difference spectra recorded between 500 and 800 nm at short delay times following pulsed excitation are dominated by features that can be attributed to stimulated emission (SE) from the lowest singlet excited state ($S_1 \rightarrow S_0$). Over time, these spectral signatures convert cleanly into broad featureless signals resulting from excited-state absorption (ESA), which persist over the entire delay time of the fs-TA experiments (7 ns). Additional experiments using ms-TA spectroscopy confirmed that these long-lived excited states of E(^{Me}PDP^{Ph})$_2$ decay back to the corresponding ground states exhibiting time constants consistent with the millisecond lifetimes determined by time-dependent emission spectroscopy. On the basis of these observations, the long-lived transient difference spectra were assigned to ESA of the lowest-energy triplet state ($T_1 \rightarrow T_n$). Further evidence for this assignment was provided by TA experiments in the presence of $^3O_2$ (Figure S16). The ms-TA data showed strong quenching of the observed ESA features reflected in significantly faster ground-state recovery and consistent with triplet excited states. In stark contrast, the spectral changes observed by fs-TA spectroscopy proved to be independent of dissolved $^3O_2$. Collectively, the TA experiments clearly indicate that the spectral evolution from SE to ESA observed by fs-TA spectroscopy directly reflects ISC from the S_1 to T_1 state in Si/Ge/Sn(^{Me}PDP^{Ph})$_2$. Kinetic modeling of the time-dependent fs-TA spectroscopic data provided time constants for the ISC process, $S_1 \rightarrow T_1$, for all three compounds (Figure 7). The observed trend shows the expected order: τ_{ISC}(Sn) = 0.25 ns < τ_{ISC}(Ge) = 1.4 ns < τ_{ISC}(Si) = 3.1 ns. This indicates faster ISC for the heavier congeners resulting in more efficient T_1 population. These data directly correlate with the extent of $^3O_2$ quenching observed by emission spectroscopy in solution. Notably, τ_{ISC} in the group 14 compounds is 1−2 orders of magnitude longer than that for the related transition metal complex Zr(^{Mes}PDP^{Ph})$_2$ (τ_{ISC} =

https://doi.org/10.1021/acs.inorgchem.2c00182
Inorg. Chem. XXXX, XXX, XXX−XXX

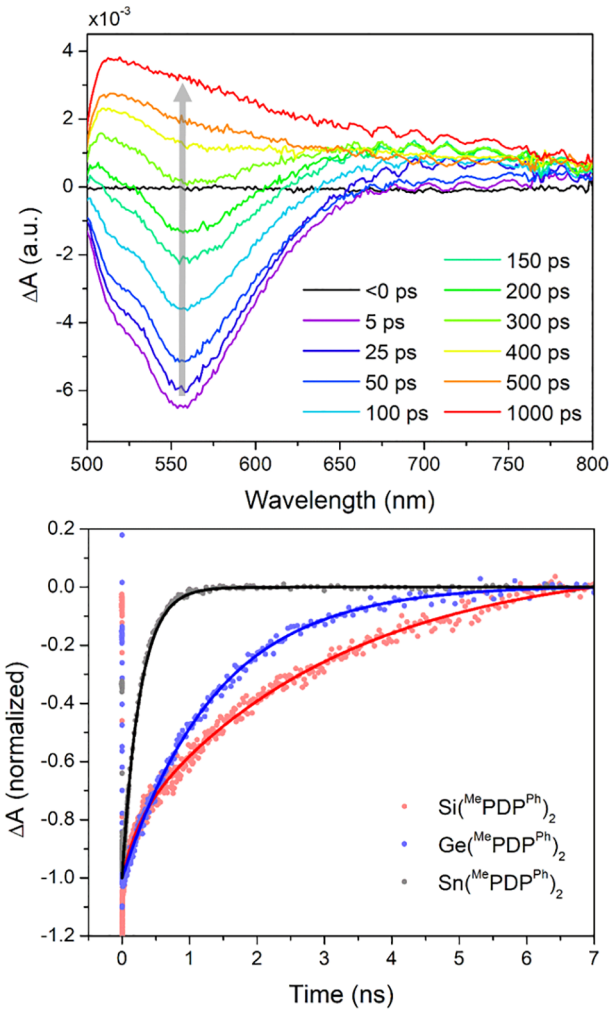

Figure 7. Femtosecond TA spectroscopic data establishing the rate constants for intersystem crossing (ISC). Time-resolved transient difference spectra (top) at selected delay times after pulsed laser excitation at 480 nm associated with the $S_1 \rightarrow T_1$ intersystem crossing process in Sn(^{Me}PDP^{Ph})$_2$; *A*, normalized absorption. Kinetic traces (bottom) for the ISC process in E(^{Me}PDP^{Ph})$_2$ (E = Si, Ge, or Sn). Solid lines represent best fits yielding the ISC rate constants provided in the text.

12.3 ps). This can be rationalized by different contributions of the heavy element to the frontier molecular orbitals of the bis-^{Me}PDP^{Ph} species. While the LUMO of Zr(^{Mes}PDP^{Ph})$_2$ exhibits substantial contributions from metal d orbitals, resulting in significant ligand-to-metal charge transfer (LMCT) contributions for the lowest-energy transitions, the very minor contributions from the group 14 elements to the same orbital in Si/Ge/Sn(^{Me}PDP^{Ph})$_2$ result in almost exclusive ligand-to-ligand (LLCT) and intraligand charge transfer character (ILCT) of the excited states. Nevertheless, the main group elements clearly play an important role in enabling TADF in these molecules, as the free H$_2$^{Me}PDP^{Ph} ligand does not exhibit long-lived emission but shows exclusively prompt fluorescence. We propose that the role of the central main group atom in facilitating ISC is twofold: (1) introduction of intramolecular heavy atom effects through small contributions of the Si, Ge, or Sn p_x and p_y orbitals to the LUMO (~2% contribution according to DFT) and (2) scaffolding of the two [^{Me}PDP^{Ph}]$^{2-}$ units in the proximity and perpendicular orientation, allowing contributions from LLCT excited states and generating a set of degenerate LUMOs (belonging to the e representation under D_{2d} symmetry) that facilitates strong SOC, respectively.

CONCLUSIONS

Our study describes a rare instance of long-lived photoluminescence in molecular compounds based on main group metals or metalloids and highlights the great potential for further discoveries in this area. The temperature-dependent steady-state emission and photoluminescence lifetime data presented herein clearly establish that emission in the three E(^{Me}PDP^{Ph})$_2$ complexes (E = Si, Ge, or Sn) occurs with excellent quantum efficiencies through a combination of prompt fluorescence and thermally activated delayed fluorescence at and around room temperature. Straightforward access to the triplet manifold is reflected in remarkably long TADF emission lifetimes in the millisecond range in solution and the direct observation of phosphorescence in frozen solution at 77 K. The efficiency of the intersystem crossing process in the new group 14 chromophores correlates strongly with the atomic number and spin−orbit coupling constant of the central element. This effect was quantified by transient absorption spectroscopy, which allowed the determination of the intersystem crossing time constants. Crucially, facile access to triplet excited states that is competitive with prompt fluorescence is observed even in Si(^{Me}PDP^{Ph})$_2$, which contains the Earth-abundant third period element silicon as the heaviest element.

Our studies also provide the rare opportunity to compare the effects of main group versus transition metal incorporation on intersystem crossing rates in otherwise isostructural chromophores. Due to the small contributions of the group 14 elements to the frontier molecular orbitals compared to related group 4 transition metal complexes, the intersystem crossing rates are significantly reduced by 1−2 orders of magnitude for the main group compounds, resulting in the observed competition between prompt and delayed fluorescence. While this complicates the detailed analysis of the TADF kinetics and excited-state dynamics for our new main group chromophores, the observed dual emission may provide new opportunities for the design of light-emitting diodes with high energy efficiency based on cheap and abundant materials.

EXPERIMENTAL DETAILS

General Considerations. All air- and moisture-sensitive manipulations were carried out using standard high-vacuum line, Schlenk, or cannula techniques or in an MBraun inert atmosphere drybox containing an atmosphere of purified nitrogen. Solvents for air- and moisture-sensitive manipulations were dried and deoxygenated using a Glass Contour Solvent Purification System and stored over 4 Å molecular sieves. Silicon tetrachloride, germanium(IV) iodide, and tin(IV) iodide were purchased from commercial sources and used without further purification. 2,6-Bis(5-methyl-3-phenyl-1*H*-pyrrol-2-yl)pyridine (H$_2$^{Me}PDP^{Ph}) was prepared as reported previously.[56] All solids were dried under high vacuum overnight to introduce them into the glovebox. Deuterated dichloromethane-d_2 for NMR spectroscopy was distilled from CaH$_2$.

Preparation of Si(^{Me}PDP^{Ph})$_2$. In the glovebox, a 50 mL Schlenk flask was charged with H$_2$^{Me}PDP^{Ph} (200 mg, 0.513 mmol) and NaH (28 mg, 1.17 mmol). Following the addition of 10 mL of THF, the flask was sealed with a rubber septum containing a syringe needle for pressure equilibration with the glovebox atmosphere. The resulting dark yellow suspension was stirred for 16 h to ensure complete

https://doi.org/10.1021/acs.inorgchem.2c00182
Inorg. Chem. XXXX, XXX, XXX−XXX

deprotonation of the ligand precursor and formation of $Na_2^{Me}PDP^{Ph}$. The reaction vessel was transferred from the glovebox to a Schlenk line, and $SiCl_4$ (44 mg, 0.26 mmol, 30 μL) was added by syringe. The reaction mixture was stirred for 8 h, resulting in a distinct change in color from dark brown to red orange. All volatiles were removed under vacuum, and the reaction vessel was returned to the glovebox. The solid residue was redissolved in THF and filtered over Celite. The red orange filtrate was concentrated to a volume of ∼10 mL under vacuum, and 15 mL of pentane was added. Cooling the solution to −35 °C overnight provided a red microcrystalline material identified as $Si(^{Me}PDP^{Ph})_2{\cdot}2THF$: yield 160 mg, 65%; ^1H NMR (400 MHz, C_6D_6) δ 7.48 (d, ^3J = 8.0 Hz, 8H, *o*-Ph*H*), 7.44−7.39 (m, 10H, *m*-Ph*H* + 4-pyridine*H*), 7.34 (t, ^3J = 6.7 Hz, 4H, *p*-Ph*H*), 7.01 (d, ^3J = 8.0 Hz, 4H, 3-pyridine*H*), 5.95 (s, 4H, 4-pyrrolide*H*), 1.75 (s, 12H, CH_3); $^{13}C\{^1H\}$ NMR (100 MHz, C_6D_6) δ 148.5, 144.7, 137.6, 137.0, 130.1, 129.7, 129.0, 127.5, 124.9, 117.3, 110.0, 12.8; HRMS (ESI) calcd for $C_{54}H_{43}N_6Si^+$ $[M + H]^+$ *m*/*z* 803.3318, found 803.3310. Anal. Calcd for $Si(^{Me}PDP^{Ph})_2{\cdot}2THF$, $C_{62}H_{58}N_6O_2Si$: C, 76.81; H, 6.03; N, 8.67. Found: C, 77.07; H, 5.70; N, 9.29. Single crystals suitable for X-ray diffraction experiments were obtained by vapor diffusion of pentane into a concentrated solution of $Si(^{Me}PDP^{Ph})_2$ in THF.

Preparation of $Ge(^{Me}PDP^{Ph})_2$. In the glovebox, a 20 mL scintillation vial was charged with $H_2^{Me}PDP^{Ph}$ (200 mg, 0.513 mmol) and NaH (28 mg, 1.17 mmol). THF (10 mL) was added to the vial, which was subsequently capped loosely. The resulting dark yellow suspension was stirred for 16 h to generate $Na_2^{Me}PDP^{Ph}$. A solution of GeI_4 (149 mg, 0.26 mmol) in THF (4 mL) was added slowly, and the reaction mixture was stirred for 8 h. The resulting suspension was filtered over Celite, and the solid residue was washed with copious amounts of THF until the washings were clear. The orange brown filtrate was concentrated to a volume of ∼10 mL under vacuum. Addition of pentane (15 mL) followed by cooling to −35 °C overnight provided an orange microcrystalline material identified as $Ge(^{Me}PDP^{Ph})_2{\cdot}2THF$: yield 185 mg, 72%; ^1H NMR (400 MHz, C_6D_6) δ 7.48 (d, ^3J = 6.9 Hz, 8H, *o*-Ph*H*), 7.43 (t, ^3J = 7.9 Hz, 8H, *m*-Ph*H*), 7.39−7.33 (m, 6H, *p*-Ph*H* + 4-pyridine*H*), 7.03 (d, ^3J = 8.0 Hz, 4H, 3-pyridine*H*), 5.98 (s, 4H, 4-pyrrolide*H*), 1.77 (s, 12H, CH_3); $^{13}C\{^1H\}$ NMR (100 MHz, C_6D_6) δ 147.9, 142.9, 139.3, 137.9, 131.4, 130.0, 129.0, 127.5, 125.5, 116.5, 112.5, 13.8; HRMS (ESI) calcd for $C_{54}H_{43}N_6Si^+$ $[M + H]^+$ *m*/*z* 849.2761, found 849.2770. Anal. Calcd for $Ge(^{Me}PDP^{Ph})_2{\cdot}2THF$, $C_{62}H_{58}GeN_6O_2$: C, 75.08; H, 5.89; N, 8.47. Found: C, 74.79; H, 5.51; N, 8.69. Single crystals suitable for X-ray diffraction experiments were obtained by vapor diffusion of pentane into a concentrated solution of $Ge(^{Me}PDP^{Ph})_2$ in dichloromethane.

Preparation of $Sn(^{Me}PDP^{Ph})_2$. In the glovebox, a 20 mL scintillation vial was charged with $H_2^{Me}PDP^{Ph}$ (200 mg, 0.513 mmol) and NaH (28 mg, 1.17 mmol). THF (10 mL) was added to the vial, which was subsequently capped loosely. The resulting dark yellow suspension was stirred for 16 h to generate $Na_2^{Me}PDP^{Ph}$. A solution of SnI_4 (162 mg, 0.26 mmol) in THF (4 mL) was added slowly, and the reaction mixture was stirred for 8 h. The resulting suspension was filtered over Celite, and the solid residue was washed with copious amounts of THF until the washings were clear. The solvent was removed in vacuum, and the orange brown residue was dissolved in a minimum amount of dichloromethane. Addition of pentane (15 mL) followed by cooling to −35 °C overnight provided an orange microcrystalline material identified as $Sn(^{Me}PDP^{Ph})_2{\cdot}3CH_2Cl_2$: yield 170 mg, 63%; ^1H NMR (400 MHz, C_6D_6) δ 7.47−7.39 (m, 16H, *o*-Ph*H* + *m*-Ph*H*), 7.36−7.28 (m, 6H, *p*-Ph*H* + 4-pyridine*H*), 6.98 (d + dd, $^3J_{H-H}$ = 8.0 Hz, $^4J_{Sn-H}$ = 11.8 Hz, 4H, 3-pyridine*H*), 6.02 (s + d, $^4J_{Sn-H}$ = 16.9 Hz, 4H, 4-pyrrolide*H*), 1.84 (s, 12H, CH_3); $^{13}C\{^1H\}$ NMR (100 MHz, C_6D_6) δ 147.9, 142.9 139.3, 137.9, 131.4, 129.9, 129.0, 127.5, 125.5, 116.5, 112.4, 13.8; HRMS (ESI) calcd for $C_{54}H_{43}N_6Si^+$ $[M + H]^+$ *m*/*z* 895.2571, found 895.2574. Anal. Calcd for $Sn(^{Me}PDP^{Ph})_2{\cdot}3CH_2Cl_2$, $C_{57}H_{48}Cl_6N_6Sn$: C, 59.61; H, 4.21; N, 7.32. Found: C, 59.40; H, 4.09; N, 6.86. Single crystals suitable for X-ray diffraction experiments were obtained by vapor diffusion of pentane into a concentrated solution of $Sn(^{Me}PDP^{Ph})_2$ in dichloromethane.

Physical Measurements. ^1H and $^{13}C\{^1H\}$ NMR spectra were recorded on an Agilent 400 MHz spectrometer, a JEOL 400 MHz YH spectrometer, or a Varian INOVA 600 MHz spectrometer. All chemical shifts are reported relative to $SiMe_4$ using ^1H (residual) chemical shifts of the solvent as a secondary standard. High-resolution mass spectra were recorded on a Thermo Finnigan Linear Trapping Quadrupole mass spectrometer. UV−vis absorption spectra were recorded on a Shimadzu UV-1800 spectrophotometer in gastight quartz cuvettes with a 10 mm path length fitted with screw caps. Emission spectra were recorded in 10 mm path length gastight quartz cuvettes with screw caps using a Shimadzu RF-5301 PC spectrofluorophotometer. Room-temperature photoluminescent decay data were collected using a Horiba Jobin Yvon Fluorolog-3 spectrofluorometer with a single photon counting module in multichannel scaler mode and a 456 nm SpectraLED pulsed excitation source. Lifetimes were determined through exponential fitting using the provided decay analysis software package, DAS version 6.1. Steady-state emission spectra from 77 to 340 K were recorded using an Oxford Instruments Optistat DN cryostat with an Edinburgh Instruments FS920 fluorimeter that was equipped with a 450 W Xe arc lamp for an excitation source and a Peltier-cooled Hamamatsu R2658P photomultiplier tube (PMT). The Oxford cryostat was also used with an Edinburgh Instruments LP920 laser flash photolysis system for which a tunable Vibrant 355 nm Nd/YAG/OPO system (Opotek) was the excitation source and a Hamamatsu R928 PMT was the detector. Ultrafast TA measurements were conducted with a 1 kHz Libra, a Ti:sapphire regenerative amplifier system (Coherent Libra), which produces an ∼800 nm pulse with ∼45 fs temporal resolution with ∼4 W power. Using a beam splitter, the output of the Libra was separated into pump and probe beam paths. The pump beam was directed to an optical parametric amplifier (Light Conversion OPerA). The optical parametric amplifier converts 800 nm Libra output into 480 nm to excite the lowest-energy transitions of $E(^{Me}PDP^{Ph})_2$ (E = Si, Ge, or Sn). The beams were directed to commercial TA spectrometers. We used Helios (Ultrafast System) and EOS (Ultrafast systems) for fs- and μs-TA, respectively. A visible-light continuum, in the ∼400−800 nm spectral region, was generated by focusing onto a Ti:sapphire crystal. Optical filters were integrated in the probe beam path for rejection of the residual, unamplified, 800 nm radiation. TA measurements were conducted under the magic angle condition where polarization of the probe is 54.7° relative to the pump. Control of the pump and probe polarizations was achieved with two sets of λ/2 waveplate and polarizer combinations placed in both pump (before the sample) and probe (before continuum generation) beam paths.

■ ASSOCIATED CONTENT

Supporting Information

The Supporting Information is available free of charge at https://pubs.acs.org/doi/10.1021/acs.inorgchem.2c00182.

Additional experimental procedures, spectroscopic and crystallographic data, and computational details (PDF)

Accession Codes

CCDC 2142966−2142968 contain the supplementary crystallographic data for this paper. These data can be obtained free of charge via www.ccdc.cam.ac.uk/data_request/cif, or by emailing data_request@ccdc.cam.ac.uk, or by contacting The Cambridge Crystallographic Data Centre, 12 Union Road, Cambridge CB2 1EZ, UK; fax: +44 1223 336033.

■ AUTHOR INFORMATION

Corresponding Authors

Carsten Milsmann − *C. Eugene Bennett Department of Chemistry, West Virginia University, Morgantown, West Virginia 26506, United States;* orcid.org/0000-0002-9249-5199; Email: camilsmann@mail.wvu.edu

https://doi.org/10.1021/acs.inorgchem.2c00182
Inorg. Chem. XXXX, XXX, XXX−XXX

Felix N. Castellano − *Department of Chemistry, North Carolina State University, Raleigh, North Carolina 27695-8204, United States;* orcid.org/0000-0001-7546-8618; Email: fncastel@ncsu.edu

Authors

Anitha S. Gowda − *C. Eugene Bennett Department of Chemistry, West Virginia University, Morgantown, West Virginia 26506, United States*

Tia S. Lee − *Department of Chemistry, Princeton University, Princeton, New Jersey 08544, United States; Department of Chemistry, North Carolina State University, Raleigh, North Carolina 27695-8204, United States;* orcid.org/0000-0003-0635-6668

Michael C. Rosko − *Department of Chemistry, North Carolina State University, Raleigh, North Carolina 27695-8204, United States;* orcid.org/0000-0001-5392-8513

Jeffrey L. Petersen − *C. Eugene Bennett Department of Chemistry, West Virginia University, Morgantown, West Virginia 26506, United States*

Complete contact information is available at: https://pubs.acs.org/10.1021/acs.inorgchem.2c00182

Notes

The authors declare no competing financial interest.

■ ACKNOWLEDGMENTS

A.S.G. and C.M. thank West Virginia University and the National Science Foundation (Grant CHE-1752738) for financial support. This work used X-ray crystallography (CHE-1336071) and NMR (CHE-1228336) instrumentation funded by the National Science Foundation. The WVU High Performance Computing facilities are funded by National Science Foundation EPSCoR Research Infrastructure Improvement Cooperative Agreement 1003907, the state of West Virginia (WVEPSCoR via the Higher Education Policy Commission), the WVU Research Corporation, and faculty investments. The work at North Carolina State University was supported by the U.S. Department of Energy, Office of Science, Office of Basic Energy Sciences, under Contract DE-SC0011979. The authors thank Prof. Gregory Scholes from Princeton University for providing access to his group's transient absorption spectrometers.

■ REFERENCES

(1) Zeitler, K. Photoredox Catalysis with Visible Light. *Angew. Chemie Int. Ed.* **2009**, *48*, 9785−9789.

(2) Tucker, J. W.; Stephenson, C. R. J. Shining Light on Photoredox Catalysis: Theory and Synthetic Applications. *J. Org. Chem.* **2012**, *77*, 1617−1622.

(3) Xuan, J.; Xiao, W.-J. Visible-Light Photoredox Catalysis. *Angew. Chemie Int. Ed.* **2012**, *51*, 6828−6838.

(4) Prier, C. K.; Rankic, D. A.; MacMillan, D. W. C. Visible Light Photoredox Catalysis with Transition Metal Complexes: Applications in Organic Synthesis. *Chem. Rev.* **2013**, *113*, 5322−5363.

(5) Monro, S.; Colón, K. L.; Yin, H.; Roque, J.; Konda, P.; Gujar, S.; Thummel, R. P.; Lilge, L.; Cameron, C. G.; McFarland, S. A. Transition Metal Complexes and Photodynamic Therapy from a Tumor-Centered Approach: Challenges, Opportunities, and Highlights from the Development of TLD1433. *Chem. Rev.* **2019**, *119*, 797−828.

(6) Zhen, X.; Qu, R.; Chen, W.; Wu, W.; Jiang, X. The Development of Phosphorescent Probes for in Vitro and in Vivo Bioimaging. *Biomater. Sci.* **2021**, *9*, 285−300.

(7) Hagfeldt, A.; Boschloo, G.; Sun, L.; Kloo, L.; Pettersson, H. Dye-Sensitized Solar Cells. *Chem. Rev.* **2010**, *110*, 6595−6663.

(8) Nazeeruddin, M. K.; Baranoff, E.; Grätzel, M. Dye-Sensitized Solar Cells: A Brief Overview. *Sol. Energy* **2011**, *85*, 1172−1178.

(9) Xu, H.; Chen, R.; Sun, Q.; Lai, W.; Su, Q.; Huang, W.; Liu, X. Recent Progress in Metal-Organic Complexes for Optoelectronic Applications. *Chem. Soc. Rev.* **2014**, *43*, 3259−3302.

(10) Ostroverkhova, O. Organic Optoelectronic Materials: Mechanisms and Applications. *Chem. Rev.* **2016**, *116*, 13279−13412.

(11) Yersin, H.; Rausch, A. F.; Czerwieniec, R.; Hofbeck, T.; Fischer, T. The Triplet State of Organo-Transition Metal Compounds. Triplet Harvesting and Singlet Harvesting for Efficient OLEDs. *Coord. Chem. Rev.* **2011**, *255*, 2622−2652.

(12) Maldotti, A. Photochemistry and Photophysics of Transition-Metal Complexes. *Photochemistry* **2009**, *37*, 240−299.

(13) Förster, C.; Heinze, K. Photophysics and Photochemistry with Earth-Abundant Metals-Fundamentals and Concepts. *Chem. Soc. Rev.* **2020**, *49*, 1057−1070.

(14) Wagenknecht, P. S.; Ford, P. C. Metal Centered Ligand Field Excited States: Their Roles in the Design and Performance of Transition Metal Based Photochemical Molecular Devices. *Coord. Chem. Rev.* **2011**, *255*, 591−616.

(15) Arias-Rotondo, D. M.; McCusker, J. K. The Photophysics of Photoredox Catalysis: A Roadmap for Catalyst Design. *Chem. Soc. Rev.* **2016**, *45*, 5803−5820.

(16) Ravinson, D. S. M.; Thompson, M. E. Thermally Assisted Delayed Fluorescence (TADF): Fluorescence Delayed Is Fluorescence Denied. *Mater. Horizons* **2020**, *7*, 1210−1217.

(17) Kalyanasundaram, K. Photophysics, Photochemistry and Solar Energy Conversion with Tris(Bipyridyl)Ruthenium(II) and Its Analogues. *Coord. Chem. Rev.* **1982**, *46*, 159−244.

(18) King, K. A.; Spellane, P. J.; Watts, R. J. Excited-State Properties of a Triply Ortho-Metalated Iridium(III) Complex. *J. Am. Chem. Soc.* **1985**, *107*, 1431−1432.

(19) Dixon, I. M.; Collin, J.-P.; Sauvage, J.-P.; Flamigni, L.; Encinas, S.; Barigelletti, F. A Family of Luminescent Coordination Compounds: Iridium(III) Polyimine Complexes. *Chem. Soc. Rev.* **2000**, *29*, 385−391.

(20) Wenger, O. S. Photoactive Complexes with Earth-Abundant Metals. *J. Am. Chem. Soc.* **2018**, *140*, 13522−13533.

(21) Larsen, C. B.; Wenger, O. S. Photoredox Catalysis with Metal Complexes Made from Earth-Abundant Elements. *Chem. - Eur. J.* **2018**, *24*, 2039−2058.

(22) Hockin, B. M.; Li, C.; Robertson, N.; Zysman-Colman, E. Photoredox Catalysts Based on Earth-Abundant Metal Complexes. *Catal. Sci. Technol.* **2019**, *9*, 889−915.

(23) Wenger, O. S. A Bright Future for Photosensitizers. *Nat. Chem.* **2020**, *12*, 323−324.

(24) Parke, S. M.; Rivard, E. Aggregation Induced Phosphorescence in the Main Group. *Isr. J. Chem.* **2018**, *58*, 915−926.

(25) Bergamini, G.; Fermi, A.; Botta, C.; Giovanella, U.; Di Motta, S.; Negri, F.; Peresutti, R.; Gingras, M.; Ceroni, P. A Persulfurated Benzene Molecule Exhibits Outstanding Phosphorescence in Rigid Environments: From Computational Study to Organic Nanocrystals and OLED Applications. *J. Mater. Chem. C* **2013**, *1*, 2717−2724.

(26) Zhao, Z.; Zheng, X.; Du, L.; Xiong, Y.; He, W.; Gao, X.; Li, C.; Liu, Y.; Xu, B.; Zhang, J.; Song, F.; Yu, Y.; Zhao, X.; Cai, Y.; He, X.; Kwok, R. T. K.; Lam, J. W. Y.; Huang, X.; Lee Phillips, D.; Wang, H.; Tang, B. Z. Non-Aromatic Annulene-Based Aggregation-Induced Emission System via Aromaticity Reversal Process. *Nat. Commun.* **2019**, *10*, 2952.

(27) Bolton, O.; Lee, K.; Kim, H. J.; Lin, K. Y.; Kim, J. Activating Efficient Phosphorescence from Purely Organic Materials by Crystal Design. *Nat. Chem.* **2011**, *3*, 205−210.

(28) Zhou, J.; Stojanović, L.; Berezin, A. A.; Battisti, T.; Gill, A.; Kariuki, B. M.; Bonifazi, D.; Crespo-Otero, R.; Wasielewski, M. R.; Wu, Y. L. Organic Room-Temperature Phosphorescence from Halogen-Bonded Organic Frameworks: Hidden Electronic Effects in Rigidified Chromophores. *Chem. Sci.* **2021**, *12*, 767−773.

(29) Yuan, W. Z.; Shen, X. Y.; Zhao, H.; Lam, J. W. Y.; Tang, L.; Lu, P.; Wang, C.; Liu, Y.; Wang, Z.; Zheng, Q.; Sun, J. Z.; Ma, Y.; Tang, B. Z. Crystallization-Induced Phosphorescence of Pure Organic Luminogens at Room Temperature. *J. Phys. Chem. C* **2010**, *114*, 6090−6099.
(30) Yoshii, R.; Hirose, A.; Tanaka, K.; Chujo, Y. Functionalization of Boron Diiminates with Unique Optical Properties: Multicolor Tuning of Crystallization-Induced Emission and Introduction into the Main Chain of Conjugated Polymers. *J. Am. Chem. Soc.* **2014**, *136*, 18131−18139.
(31) Gong, Y.; Zhao, L.; Peng, Q.; Fan, D.; Yuan, W. Z.; Zhang, Y.; Tang, B. Z. Crystallization-Induced Dual Emission from Metal- and Heavy Atom-Free Aromatic Acids and Esters. *Chem. Sci.* **2015**, *6*, 4438−4444.
(32) Xue, P.; Sun, J.; Chen, P.; Wang, P.; Yao, B.; Gong, P.; Zhang, Z.; Lu, R. Luminescence Switching of a Persistent Room-Temperature Phosphorescent Pure Organic Molecule in Response to External Stimuli. *Chem. Commun.* **2015**, *51*, 10381−10384.
(33) Zhao, J.; Chen, K.; Hou, Y.; Che, Y.; Liu, L.; Jia, D. Recent Progress in Heavy Atom-Free Organic Compounds Showing Unexpected Intersystem Crossing (ISC) Ability. *Org. Biomol. Chem.* **2018**, *16*, 3692−3701.
(34) Tilley, A. J.; Pensack, R. D.; Lee, T. S.; Djukic, B.; Scholes, G. D.; Seferos, D. S. Ultrafast Triplet Formation in Thionated Perylene Diimides. *J. Phys. Chem. C* **2014**, *118*, 9996−10004.
(35) Palmer, J. R.; Wells, K. A.; Yarnell, J. E.; Favale, J. M.; Castellano, F. N. Visible-Light-Driven Triplet Sensitization of Polycyclic Aromatic Hydrocarbons Using Thionated Perinones. *J. Phys. Chem. Lett.* **2020**, *11*, 5092−5099.
(36) Pristash, S. R.; Corp, K. L.; Rabe, E. J.; Schlenker, C. W. Heavy-Atom-Free Red-to-Yellow Photon Upconversion in a Thiosquaraine Composite. *ACS Appl. Energy Mater.* **2020**, *3*, 19−28.
(37) Webster, S.; Peceli, D.; Hu, H.; Padilha, L. A.; Przhonska, O. V.; Masunov, A. E.; Gerasov, A. O.; Kachkovski, A. D.; Slominsky, Y. L.; Tolmachev, A. I.; Kurdyukov, V. V.; Viniychuk, O. O.; Barrasso, E.; Lepkowicz, R.; Hagan, D. J.; Van Stryland, E. W. Near-Unity Quantum Yields for Intersystem Crossing and Singlet Oxygen Generation in Polymethine-like Molecules: Design and Experimental Realization. *J. Phys. Chem. Lett.* **2010**, *1*, 2354−2360.
(38) Nguyen, V. N.; Qi, S.; Kim, S.; Kwon, N.; Kim, G.; Yim, Y.; Park, S.; Yoon, J. An Emerging Molecular Design Approach to Heavy-Atom-Free Photosensitizers for Enhanced Photodynamic Therapy under Hypoxia. *J. Am. Chem. Soc.* **2019**, *141*, 16243−16248.
(39) Xu, J.; Takai, A.; Kobayashi, Y.; Takeuchi, M. Phosphorescence from a Pure Organic Fluorene Derivative in Solution at Room Temperature. *Chem. Commun.* **2013**, *49*, 8447−8449.
(40) Kremer, A.; Aurisicchio, C.; Deleo, F.; Ventura, B.; Wouters, J.; Armaroli, N.; Barbieri, A.; Bonifazi, D. Walking Down the Chalcogenic Group of the Periodic Table: From Singlet to Triplet Organic Emitters. *Chem. - Eur. J.* **2015**, *21*, 15377−15387.
(41) Kang, Y.; Song, D.; Schmider, H.; Wang, S. Novel Blue Phosphorescent Group 15 Compounds MR_3 (M = P, Sb, Bi; R = p-(N-7-Azaindolyl)Phenyl). *Organometallics* **2002**, *21*, 2413−2421.
(42) Jia, W. L.; Liu, Q. De; Wang, R.; Wang, S. Novel Phosphorescent Cyclometalated Organotin(IV) and Organolead(IV) Complexes of 2,6-Bis(2′-Indolyl)Pyridine and 2,6-Bis[2′-(7-Azaindolyl)]Pyridine. *Organometallics* **2003**, *22*, 4070−4078.
(43) Strasser, A.; Vogler, A. Optical Properties of Thallium(I), Lead(II) and Bismuth(III) Hexafluoroacetylacetonates. Intraligand Phosphorescence under Ambient Conditions. *Inorg. Chem. Commun.* **2004**, *7*, 528−530.
(44) Strasser, A.; Vogler, A. Intraligand Phosphorescence of Lead(II) β-Diketonates under Ambient Conditions. *J. Photochem. Photobiol. A Chem.* **2004**, *165*, 115−118.
(45) Gouterman, M.; Schwarz, F. P.; Smith, P. D.; Dolphin, D. Porphyrins. XXVII. Spin-Orbit Coupling and Luminescence of Group IV Complexes. *J. Chem. Phys.* **1973**, *59*, 676−690.
(46) Endo, A.; Ogasawara, M.; Takahashi, A.; Yokoyama, D.; Kato, Y.; Adachi, C. Thermally Activated Delayed Fluorescence from Sn4+-Porphyrin Complexes and Their Application to Organic Light-Emitting Diodes -A Novel Mechanism for Electroluminescence. *Adv. Mater.* **2009**, *21*, 4802−4806.
(47) Maeda, D.; Shimakoshi, H.; Abe, M.; Hisaeda, Y. Syntheses and Photophysical Behavior of Porphyrin Isomer Sn(IV) Complexes. *Inorg. Chem.* **2009**, *48*, 9853−9860.
(48) Toma, O.; Mercier, N.; Allain, M.; Meinardi, F.; Botta, C. Lead(II) 4,4′-Bipyridine N-Oxide Coordination Polymers - Highly Phosphorescent Materials with Mechanochromic Luminescence Properties. *Eur. J. Inorg. Chem.* **2017**, *2017*, 844−850.
(49) Wang, Z. P.; Wang, J. Y.; Li, J. R.; Feng, M. L.; Zou, G. D.; Huang, X. Y. $[Bmim]_2SbCl_5$: A Main Group Metal-Containing Ionic Liquid Exhibiting Tunable Photoluminescence and White-Light Emission. *Chem. Commun.* **2015**, *51*, 3094−3097.
(50) Toma, O.; Allain, M.; Meinardi, F.; Forni, A.; Botta, C.; Mercier, N. Bismuth-Based Coordination Polymers with Efficient Aggregation-Induced Phosphorescence and Reversible Mechanochromic Luminescence. *Angew. Chemie Int. Ed.* **2016**, *55*, 7998−8002.
(51) Parke, S. M.; Hupf, E.; Matharu, G. K.; de Aguiar, I.; Xu, L.; Yu, H.; Boone, M. P.; de Souza, G. L. C.; McDonald, R.; Ferguson, M. J.; He, G.; Brown, A.; Rivard, E. Aerobic Solid State Red Phosphorescence from Benzobismole Monomers and Patternable Self-Assembled Block Copolymers. *Angew. Chemie Int. Ed.* **2018**, *57*, 14841−14846.
(52) He, G.; Torres Delgado, W.; Schatz, D. J.; Merten, C.; Mohammadpour, A.; Mayr, L.; Ferguson, M. J.; McDonald, R.; Brown, A.; Shankar, K.; Rivard, E. Coaxing Solid-State Phosphorescence from Tellurophenes. *Angew. Chemie Int. Ed.* **2014**, *53*, 4587−4591.
(53) He, G.; Wiltshire, B. D.; Choi, P.; Savin, A.; Sun, S.; Mohammadpour, A.; Ferguson, M. J.; McDonald, R.; Farsinezhad, S.; Brown, A.; Shankar, K.; Rivard, E. Phosphorescence within Benzotellurophenes and Color Tunable Tellurophenes under Ambient Conditions. *Chem. Commun.* **2015**, *51*, 5444−5447.
(54) Braun, C. A.; Zomerman, D.; De Aguiar, I.; Qi, Y.; Delgado, W. T.; Ferguson, M. J.; McDonald, R.; De Souza, G. L. C.; He, G.; Brown, A.; Rivard, E. Probing the Nature of Peripheral Boryl Groups within Luminescent Tellurophenes. *Faraday Discuss.* **2017**, *196*, 255−268.
(55) Torres Delgado, W.; Braun, C. A.; Boone, M. P.; Shynkaruk, O.; Qi, Y.; McDonald, R.; Ferguson, M. J.; Data, P.; Almeida, S. K. C.; de Aguiar, I.; De Souza, G. L. C.; Brown, A.; He, G.; Rivard, E. Moving beyond Boron-Based Substituents to Achieve Phosphorescence in Tellurophenes. *ACS Appl. Mater. Interfaces* **2018**, *10*, 12124−12134.
(56) Zhang, Y.; Petersen, J. L.; Milsmann, C. A Luminescent Zirconium(IV) Complex as a Molecular Photosensitizer for Visible Light Photoredox Catalysis. *J. Am. Chem. Soc.* **2016**, *138*, 13115−13118.
(57) Zhang, Y.; Lee, T. S.; Petersen, J. L.; Milsmann, C. A Zirconium Photosensitizer with a Long-Lived Excited State: Mechanistic Insight into Photo-Induced Single Electron Transfer. *J. Am. Chem. Soc.* **2018**, *140*, 5934−5947.
(58) Zhang, Y.; Petersen, J. L.; Milsmann, C. Photochemical C-C Bond Formation in Luminescent Zirconium Complexes with CNN Pincer Ligands. *Organometallics* **2018**, *37*, 4488−4499.
(59) Zhang, Y.; Akhmedov, N. G.; Petersen, J. L.; Milsmann, C. Photoluminescence of Seven-Coordinate Zirconium and Hafnium Complexes with 2,2'-Pyridylpyrrolide Ligands. *Chem. - Eur. J.* **2019**, *25*, 3042−3052.
(60) Zhang, Y.; Leary, D. C.; Belldina, A. M.; Petersen, J. L.; Milsmann, C. Effects of Ligand Substitution on the Optical and Electrochemical Properties of (Pyridinedipyrrolide)Zirconium Photosensitizers. *Inorg. Chem.* **2020**, *59*, 14716−14730.
(61) Zhang, Y.; Lee, T. S.; Favale, J. M.; Leary, D. C.; Petersen, J. L.; Scholes, G. D.; Castellano, F. N.; Milsmann, C. Delayed Fluorescence from a Zirconium(IV) Photosensitizer with Ligand-to-Metal Charge-Transfer Excited States. *Nat. Chem.* **2020**, *12*, 345.

https://doi.org/10.1021/acs.inorgchem.2c00182
Inorg. Chem. XXXX, XXX, XXX−XXX

(62) Dias, F. B.; Bourdakos, K. N.; Jankus, V.; Moss, K. C.; Kamtekar, K. T.; Bhalla, V.; Santos, J.; Bryce, M. R.; Monkman, A. P. Triplet Harvesting with 100% Efficiency by Way of Thermally Activated Delayed Fluorescence in Charge Transfer OLED Emitters. *Adv. Mater.* **2013**, *25*, 3707−3714.
(63) Data, P.; Pander, P.; Okazaki, M.; Takeda, Y.; Minakata, S.; Monkman, A. P. Dibenzo[a,j]Phenazine-Cored Donor-Acceptor-Donor Compounds as Green-to-Red/NIR Thermally Activated Delayed Fluorescence Organic Light Emitters. *Angew. Chemie Int. Ed.* **2016**, *55*, 5739−5744.

https://doi.org/10.1021/acs.inorgchem.2c00182
Inorg. Chem. XXXX, XXX, XXX−XXX